

How to find long quasi-monochromatic gravitational wave transients with unknown frequency evolution?

Péter Raffai, Zsolt Frei

Institute of Physics, Eötvös University, Pázmány P. s. 1/A, 1117 Budapest, Hungary

Zsuzsa Márka, Szabolcs Márka

Columbia University, Pupin Laboratories, New York, NY 10027

Abstract.

We present two general methods, the so-called Locust and the generalized Hough algorithm, to search for quasi-monochromatic signals of moderate frequency evolution and limited duration in datastreams of gravitational wave detectors. Some models of long gamma ray bursts (e.g. van Putten, 2003) predict quasi-monochromatic gravitational wave signals of limited duration emitted during the gamma ray burst event. These type of signals give rise to curling traces of local maxima in the time-frequency space that can be recovered via image processing methods (Locust and Hough). Tests of the algorithms in the context of the van Putten model were carried out using injected simulated signals into gaussian white noise and also into LIGO-like data. The Locust algorithm has the relative advantage of having higher speed and better general sensitivity, however, the generalized Hough algorithm is more tolerant of trace discontinuities. Combination of the two algorithms increases search robustness and sensitivity at the price of execution speed.

Submitted to: *Class. Quantum Grav.*

PACS numbers: 04.80.Nn, 07.05.Kf, 95.85.Sz

1. Introduction

Quasi-monochromatic gravitational waves (GWs) are one of the types of signals that are expected to be detectable by ground-based interferometric detectors [1], such as LIGO [2, 3], VIRGO [4], TAMA300 [5], and GEO600 [6]. Known possible sources of these type of signals include rotating non-axisymmetric or oscillating neutron stars [7, 8]. The long duration and known frequency evolution of their expected signals allows for integration on long time scales, thus signals (in principle) can be detected at very small signal-to-noise ratios. The motion of Earth (rotation and orbital motion around the Sun) modulate long duration GW signals, which for known source sky positions can be taken into account. However, in case of a blind search, where source position is unknown, the size of the parameter space becomes so large that search processes based on long-term integration are limited by present computational capabilities. One must face similar difficulties if frequency evolution and/or time duration of signals are unknown.

Methods used in searches for quasi-monochromatic GW signals with interferometric detectors so far were based on coherent integration of data [9], or include matched filtering [10], the Stack Slide method [11, 12] or linear Hough transformation ([13, 14, 15] and recently [16, 17, 18]). These methods usually do targeted searches and/or take advantage of the known evolution of signal frequency and hourly-monthly duration of searched signals.

In this paper we examine methods capable of detecting signals with unknown frequency evolution and limited duration. We will illustrate the techniques through a plausible astrophysical prediction. Gravitational waves are expected to be emitted during long gamma-ray burst events, lasting for $\sim 2 - 100$ s [19, 20, 21, 22, 23]. An alternative model of long gamma ray bursts [24, 25] (GRBs) predicts quasi-monochromatic gravitational wave emission lasting for a few tens of seconds during the GBR event, instead of a short transient. The model assumes the source of the radiation to be a magnetically interacting system of a rapidly rotating Kerr black hole surrounded by a uniformly magnetized rotating torus and a remnant stellar envelope. A significant portion of the GRB's energy is emitted by the torus in form of GW radiation. The model predicts the emission of $T \simeq 90$ s long GW signal for $7M_{\odot}$ mass black hole, corresponding to the lifetime of the black hole spin. Event rate is predicted to be ~ 1 per year within a distance of 100 Mpc. Nominal frequency of the GW signal is predicted to be around $f_{GW} \simeq 500$ Hz and scales as

$$f_{GW} \simeq 500 \left(\frac{\eta}{0.1} \right) \left(\frac{7M_{\odot}}{M_H} \right) \text{ Hz}, \quad (1)$$

where M_H is the mass of the Kerr black hole, and η is the ratio of angular velocities of the torus and the Kerr black hole. However, the GW signal frequency is expected to vary slowly with time by a total variation within signal duration of $\lesssim 10\%$.

The rotation of the torus around the black hole can be modulated by a precessing motion (Lense-Thirring precession, [26]) that also modulates the GW signal. Angular velocity of this precession is typically around $\simeq 10\%$ of the angular velocity of the

rotating motion of the torus.

GW signal features proposed in this model will be used to illustrate the strengths and limitations of the search methods. For timescales of a few tens of seconds long-term variations, such as tidal effects, rotation of the Earth, motion of the Earth around the Sun, etc, do not appreciably affect the signal. The restriction we impose on the frequency evolution of the function representing a signal is the slow variance of frequency with time.

We present two algorithms ("Locust" and generalized "Hough") that are capable of searching for quasi-monochromatic signals, in general. The Locust algorithm uses local wandering, while the Hough algorithm implements the Hough transformation method[27], while providing a generalization such that polynomial curves, not just straight lines, can be fitted. While tests of the methods were carried out using characteristic signal forms, durations and frequency drifts predicted by the van Putten model of GRBs, we would like to point out that in principle both methods require minimal assumptions about the GW waveform beyond its duration, relatively narrow frequency content and frequency evolution describable with polynomials.

We give a description of the two algorithms as applied in a single detector datastream process, and results of corresponding sensitivity tests in sec.2 and sec.3, respectively. Test results for multiple datastream processing are presented in sec.4.

2. Search Method

The pipeline starts with filtering a finite stretch of input data. Then we create a spectrogram of the data stretch by applying discrete Fourier-transformation. The spectrogram is then flattened by normalizing each of its rows separately. Finally, one or both of the image processing methods (Locust and the generalized Hough method) is applied to find traces of local maxima corresponding to signals. In this section a detailed description of each step of the pipeline from filtering to the image processing methods is given.

2.1. Transformation of Data into Time-Frequency Space

First the time-amplitude data stream of a single gravitational wave detector is divided into T_{seg} second long 50% overlapping segments. Taking the van Putten model as a basis, we chose T_{seg} to be $T = 10 s$. Such segment length provides reasonable search resolution while being a significant fraction of the tens of seconds duration of the long gamma ray burst signals predicted by the model. However, parameter T_{seg} is to be optimized if faster frequency evolution or significantly different signal duration is expected.

2.1.1. Filtering Filtering of input data with respect to the LIGO detectors' spectral sensitivity [28] is performed (IIR, Butterworth bandpass filter in the 80 – 2000 Hz range). At certain frequencies narrow "insensitivity" peaks (power lines, violin mode of mirror suspension, calibration lines, etc.) appear in the spectral sensitivity curve

of LIGO detectors which are also eliminated by notch filtering in the time-domain. Filtering in the time domain has the advantage of enabling us to cut out only the narrow peaks from the spectrum without touching the wider frequency environment of Fourier transformation bins and mitigate energy bleeding into other frequency bins.

All filtering procedures were performed via zero-phase means [29] in order to facilitate coherent processing afterwards. Finally $T_{trans} = 2.5$ s long segments (based on numerical studies of filters) were cut off from the beginning and end of the originally $T_{seg} = 10$ s long data segment to remove filter transients, leaving $T = 5$ s for further processing.

2.1.2. Discrete Fourier-transformation After filtering, a discrete Fourier-transformation is used to transform the time-amplitude sample into a two-dimensional time-frequency space. In the transform process a Tukey window [30] is used, where the ratio of taper to constant sections is 0.5. The sample is split into overlapping sections of size equal to the size of the window: the overlap between neighboring segments is 1/4 of the window size. After the transformation of the data, only the relevant frequency range that is compatible with the range of the bandpass filter (i.e. 80 – 2048 Hz) is processed further.

In case of processing the datastream of a single detector, we take the absolute value of every element in the resulting matrix of Fourier-coefficients. As a result, we get a matrix of non-negative real elements. The rows of this matrix represent the frequency while columns the time axis of the Fourier-space.

2.1.3. Spectrum Flattening Filtering and detector response presents the data such that certain frequency regions get overemphasized or deemphasized. This effect is transferred into the Fourier-coefficient matrix, thus its rows need to be normalized with respect to each other. Hereafter, we refer to this normalization process as "flattening". This procedure produces similar results to "whitening" generally applied during the filtering phase for other methods [31].

If a filtered data sample only consists of random noise and does not contain contributions from a real signal, then we empirically found the magnitude of the Fourier-coefficients in each row to be well described by a gamma distribution. In the case of signal presence in the data, the resulting distribution of coefficients is altered from this gamma distribution in the range of the highest values.

One can identify segments of data that are expected to have very similar frequency content but is not expected to have signal contribution. For example, for triggered searches, such off-source segments are typically chosen outside of the trigger window but still from the same detector lock stretch where the data frequency characteristics are alike. We apply the gamma function fit to rows of spectrograms that belong to such "off-source" data segments. Therefore the average and sigma that is used in the flattening process are deduced from different spectrograms that are shifted in time compared to the spectrogram to be flattened.

The final step of flattening is the subtraction of this average from every element of the row and the division of the row by sigma. This procedure essentially takes away the fraction of power in the given frequency bin that is associated with the "average" noise (noise power removal). This flattening process is done for every row of the matrix separately. In this paper from now on we will refer to the resulting flattened Fourier-coefficient matrix as "spectrogram".

2.2. Image Processing Algorithms

A generalized quasi-monochromatic signal in the input data will manifest itself as a trace consisting of a chain of local maxima in the time-frequency space. This can be described as a polynomial function of time. Our goal is to find and identify these traces in the noisy background. We treat the two-dimensional time-frequency space as a grayscale image, for which the shade of a pixel is proportional to the magnitude of the corresponding matrix element (i.e. excess energy), thus signal search task is converted into an image processing problem. We have used two independent algorithms in image analysis: the so called Locust algorithm (conceived by us), and a method based on the generalized Hough-transform.

2.2.1. The Locust Algorithm The method is based on a gradient driven wandering. Traces of local maxima to be identified in the spectrogram image of the input data consists of loosely connected chains of non-negative elements.

The simplest way to describe the actual algorithm scheme is through the next analogy: in a grayscale image we are searching for a trace of local maxima via a path that resembles that of a virtual "locust" (thus we call it "Locust algorithm"). This metaphoric "insect" crossing through a "virtual cropfield" (i.e. the grayscale image of the spectrogram) looks for the maximum of "grain" (i.e. Fourier coefficients) in its local environment.

Its local environment is described by $n \times m$ time-frequency bins, first heading forward, then backward along the time axis, from the same starting point. The starting point of the "locust" is always the absolute maximum of the processed spectrogram (which is reduced to zero immediately). It searches for the maximum in its local environment heading forward in time, jumps to local maximum found, and reduces its value to zero ("eats up the grain in that bin of the cropfield"). It then looks for the next maximum similar way until it either reaches the edge of the image or at any time the maximum in a local environment is found to be zero. The wandering is then repeated the same way, but heading backward in time from the original starting point.

Such forward-backward path pairs of the "locust" represents one trace of local maxima we are looking for. If the ratio of the sum over the number of elements in the integral for a given trace exceeds the value of a preset threshold, the search results in an alarm and the properties of the trace are saved. The Locust search then continues from the next absolute maximum of the matrix, until every element of the matrix are

reduced to zero.

The final step of the Locust search visualizes saved traces, first separately, then together in one image. All trace elements are added to a null-matrix of same size as the spectrogram, and a polynomial curve of given order is fitted to elements of this resulting matrix. The parameters of the polynomial fit are determined via minimization of the distance of the fit from the trace pixel element positions, weighted by the actual grayscale shade (that is significance of the given time-frequency bin) of each pixel. Knowing the parameters of the polynomial curve having the best fit to the traces allows us to give an estimate on the properties of the GW source in the context of the applied model of long GRBs.

An example for resulting images of Locust search is shown in fig.(1).

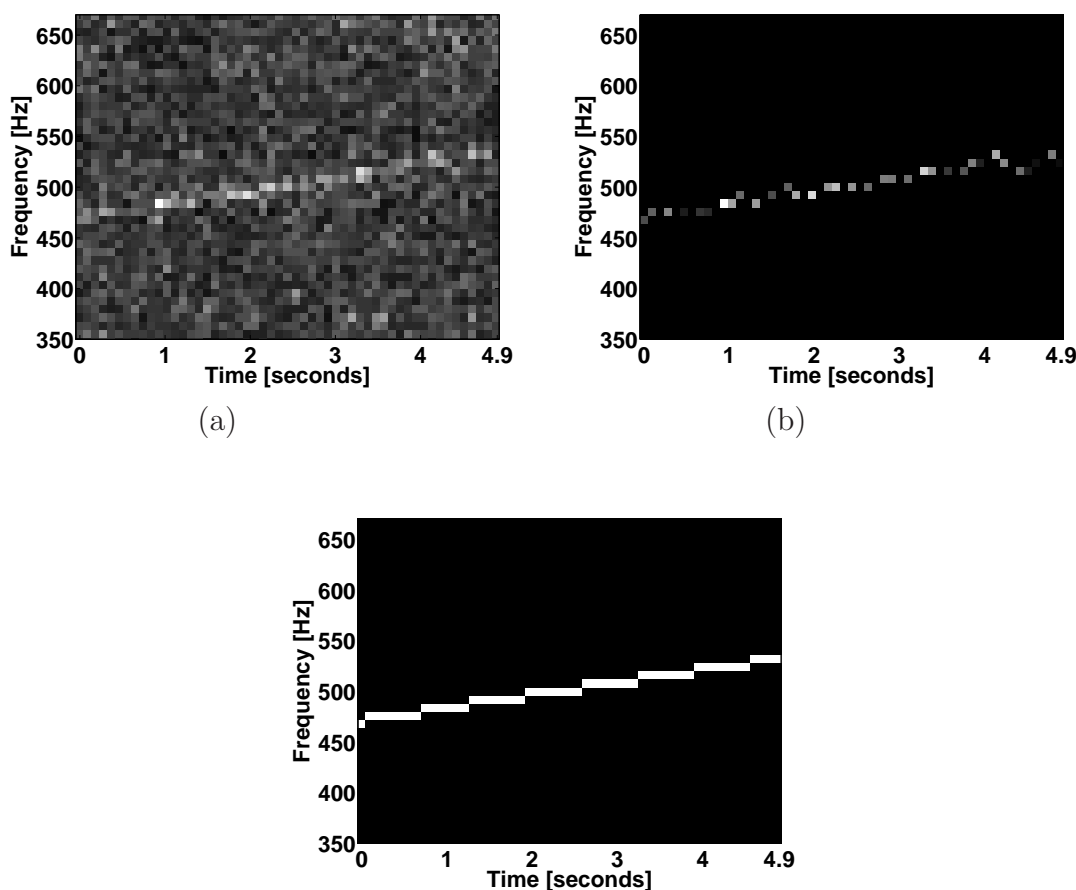


Figure 1. Pre-processed spectrogram of input data in the local frequency environment of injected signal (a). Plot of a trace satisfying the alarm requirements of the Locust method (b). A second order polynomial curve fitted to the above trace found by Locust method (c).

2.3. The Generalized Hough Algorithm

This is a generalization of the Hough-transform method [27] and is based on polynomial curve fitting to a trace of local maxima instead of the traditional line. First a dimension parameter (D) is chosen representing the dimension of the space of polynomial parameters. In most implementations of the Hough transform only linear fits are considered ($D = 2$). We shall consider higher order polynomials. For a given dimension parameter, D number of positive elements from the spectrogram are selected and a polynomial curve of $D - 1$ order is fitted to them. This procedure continues for other D number of positive elements from the spectrogram until every combination of positive elements are taken into account.

This process results in an 'output matrix' of D columns and $\binom{N}{D}$ - the number of different combinations - rows, where N is the total number of positive elements in the matrix. Each row of this 'output matrix' contain polynomial fit parameters that describe a position vector of a single datapoint in the "Hough space" (essentially a D -dimensional polynomial parameter space). If a signal is present in the input data, and its frequency evolution can be described by a polynomial function of order $D - 1$, the resulting data points in the "Hough space" have an extremely high density within a small parameter region. To identify this high density region, we collect data points in histogram bins for each parameter, and look for the bin that contains the most data points. Binsize was chosen to be such as to minimize the probability for multiple datapoints to be in one bin for an approximately homogeneous density distribution (i.e. in the absence of a signal in input data), while still get an appreciable resolution for the histogram. We choose final parameters of the polynomial (and thus the best fit to the signal trace) to be equal to the components of the position vector that points to the closest datapoint to the center of mass of the bin with the highest number of datapoints. The Hough search process then results in an alarm if the ratio of the sum of Fourier-coefficients in the 1 bin local frequency environment along the found polynomial trace, over the number of these coefficients, exceed a predefined threshold.

An example for the binned parameter space in the proximity of the density maximum is shown in fig.(2).

Execution time of the Hough process is proportional to N^D . In order to save running time, we can reduce N , the number of positive elements in the spectrogram. Because Fourier-coefficients with the highest values have the highest probability to belong to a trace corresponding to a potential signal, we keep a certain number of elements with the highest value and reduce value of the rest of the elements to zero. In our tests, we chose this number to be 15. The number of elements to be left untouched was and can be optimized to a limit that our false alarm rate and execution speed tolerance requirement allows.

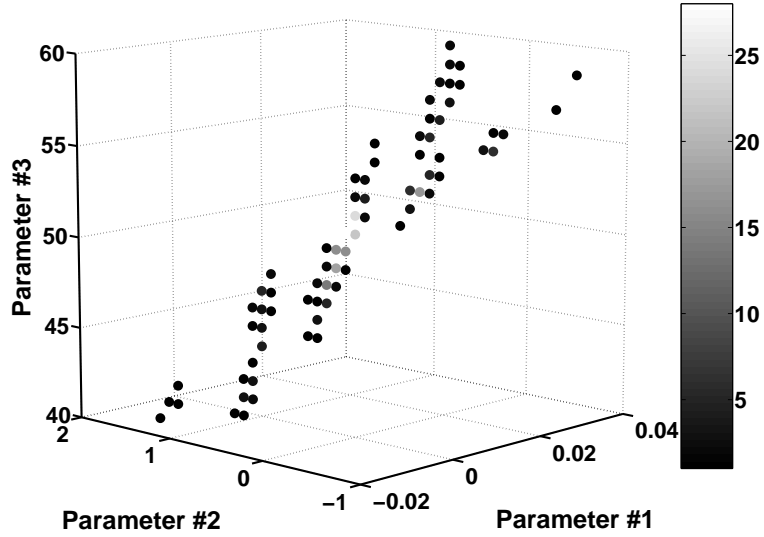


Figure 2. Three dimensional binned Hough parameter space (corresponding to second order polynomials fitted to traces of local maxima in the spectrogram), in proximity of the density maximum. Shade of markers represent the number of datapoints in the appropriate bins. Parameters of the best fit are chosen to correspond to the closest datapoint to the center of mass of the bin with the highest number of datapoints.

2.4. Comparison of Locust and Hough algorithms

The characteristic features of traces for which Locust and Hough methods are the most sensitive differ in many aspects.

Terms of alarm in the Locust method are independent from the length of the trace and all traces of a spectrogram satisfying alarm conditions are treated as parts of one trace with discontinuities. However, the alarm rate for the Locust algorithm drops if the trace corresponding to a signal has significant discontinuities beyond the $\Delta f \times \Delta t$ size of the local environment of the search. In that case the Locust search chooses a maximum from the noise background and might continue the process by following local noise maxima. Thus the final trace may not reach the threshold level for alarm even if it contains segmental contributions of a real signal. This effect is more likely at low signal-to-noise ratios, and can be reduced by optimizing the size of the local environment applied in the Locust maximum search to the expected signal-to-noise ratios.

Compared to the Hough method, the Locust method has the relative advantage of higher execution speed and its performance in principle is less dependent from the order of the polynomial to be fitted to the identified traces (somewhat independent from the signal waveform).

Alarm rate of the Hough search process is less dependent on trace discontinuities, however it is highly dependent on the order of the polynomial to be fit (D-1). Increasing D leads to an exponentially greater computational time. This can be partially compensated by decreasing the number of non-zero elements used in the

Hough transform, which saves execution time, however decreases number of alarms and increases false alarm rate.

Because of their differing response to the choice of signal trace polynomial fit and to trace discontinuities, a combination of the two independent methods (Locust and generalized Hough) in one search process can lead to higher sensitivity with a cost of greater computational time. The easiest way to combine the two algorithms in one process is applying both of them paralelly on the same datastream, and take the union of their outputs.

3. ROC-tests

The sensitivity of our search methods was tested by finding the alarm rate versus false alarm rate (i.e. the receiver operating curve or ROC) for injected signals into simulated noise.

We have completed our tests for two types of noise; gaussian white noise and a LIGO-like data with basic statistical characteristics (e.g. amplitude distribution, spectral compatibility) of LIGO 4 km detectors during the 4th science run [32]. To calculate the alarm and false alarm rates, we used 500 samples from gaussian and 250 samples from LIGO-like noise, all are 10 s long.

Gravitational wave signals ($h(t)$) can be expressed as linear combinations of signals of two independent polarizations:

$$h(t) = F_+ h_+(t) + F_\times h_\times(t) \quad (2)$$

where F_+ and F_\times are linear coefficients dependent on the detector's directional sensitivity characteristics and the position of the source in the sky.

In the van Putten model [24] $h_+(t)$ and $h_\times(t)$ are expressed as

$$h_+(t) = A \times (1 + l(t)^2) \times \cos(2 \times \Omega_T(t) \times t) \quad (3)$$

and

$$h_\times(t) = -2 \times A \times l(t) \times \sin(2 \times \Omega_T(t) \times t). \quad (4)$$

In these expressions A is the amplitude of the GW signal while the time-dependent geometrical factor, $l(t)$, and the angular velocity of the torus in the van Putten model[24], $\Omega_T(t)$, are functions of time:

$$l(t) = B \times \cos(\Omega_{LT}(t) \times t) + D \quad (5)$$

where $\Omega_{LT}(t)$ is the angular velocity of the potential Lense-Thirring precession of the torus, while B , D are other variables dependent on the properties of the source and parameters of its motion (see [24, 23] for details).

In general, Ω_T can be any kind of continuous function of time, but in our analysis the simplest, but still not trivial, case of second order polynomials were considered. Since our analysis is carried out in time-frequency space and the functions that describe the frequency evolution of GW signals are the same for both polarizations, search sensitivity

and test results are the same for signal functions of both kind. For this reason, the results are given only for $h_+(t)$.

As it is seen in eq.(5), a possible Lense-Thirring precession of the torus might modulate the van Putten signal with a cosine function of frequency Ω_{LT} . This causes sidebands to appear in the spectrum of the signal at frequencies $2\Omega_T + \Omega_{LT}$ and $2\Omega_T - \Omega_{LT}$. According to predictions of the van Putten model [24], Ω_{LT} typically does not exceed the nominal value of $\simeq 0.1\Omega_T$ [24]. We chose frequency resolution of our demonstration (8 Hz/bin) such that modulation sidebands usually do not appear in separate frequency bins from the main trace of the signal. Possible slight broadening of the main trace however can be handled by both Locust and Hough algorithms.

The Locust algorithm results with an alarm, if the ratio of the integral and the number of elements of a trace exceeds a given threshold, C . In case of the Hough method, the same ratio is calculated and compared to a predefined threshold, C , but integration is carried out for the 1 bin local frequency environment along the polynomial curve found by method.

To map ROC characteristics of a method, one first needs to explore the alarm and the false alarm rate as a function of threshold C . Using gaussian white noise and LIGO-like noise samples without injections (all going through identical processing described in section 2.1), we applied the Locust and Hough methods. The distribution results then directly gives us the false alarm rate (FAR) as a function of C . We follow the same method, but with injection of van Putten type signals (eq.(3)) to find the alarm rate for the same C threshold values. Each point on the ROC curves is then produced by identifying the C threshold value for a given false alarm rate from the FAR vs. C empirical curve and then finding the alarm rate corresponding to the same C threshold using the alarm rate vs. C curve. At extremely low FARs and alarm rates linear extrapolation to the log-log tail of the empirical FAR (or alarm rate) vs. C curves was used.

The resulting ROC-curves of the Locust and Hough methods, for four different signal root sum square amplitudes (i.e. $hrss = \sqrt{\int h(t)^2 dt}$, [33]) in the $hrss = 6.3 \times 10^{-21} - 2.1 \times 10^{-20} 1/\sqrt{Hz}$ range are given in fig.(3). The corresponding LIGO-like data noise sensitivity in the 400-600 Hz region (corresponding to the injected van Putten type signal's frequency content) is $\sim 3.8 \times 10^{-22} 1/\sqrt{Hz}$. For gaussian white noise data (mean=0, sigma=1) the injected hrss-s range is $6.6 \times 10^{-2} - 2.2 \times 10^{-1} 1/\sqrt{Hz}$.

4. Processing datastreams of multiple detectors

As an obvious generalization, we can increase search sensitivity via coherent use of data streams of multiple interferometers, and process the resulting single stream with the Locust and Hough methods. If the time delay between the realization of the same signal in different data streams is well known, the data streams can be synchronized by shifting one of the streams relatively to the other by the known delay. Additionally the detectors' orientation with respect to each other and the proposed source direction (i.e.

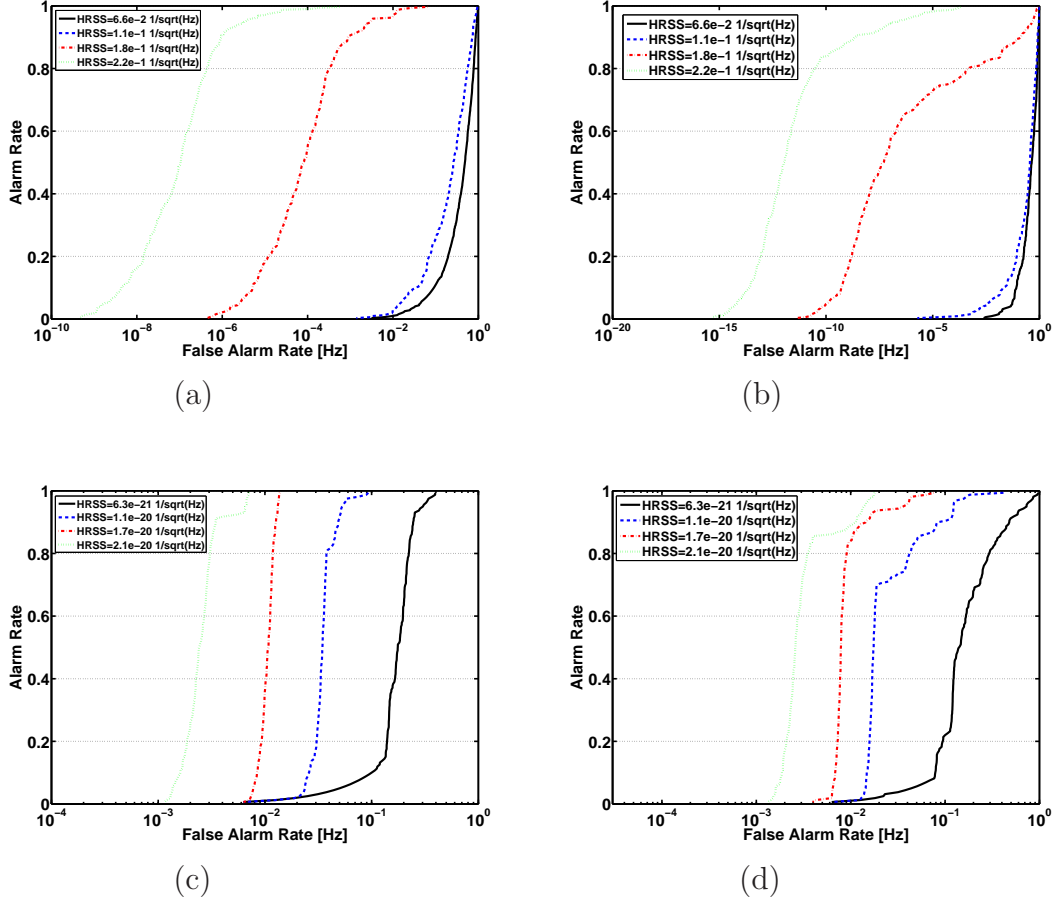


Figure 3. ROC curves of single datastream searches. a:white noise/Locust, b:white noise/Hough, c:modified LIGO/Locust, d:modified LIGO/Hough.

the antenna factors) can also be taken into account.

We will illustrate the simplest case where sky position is known (optimal) and the detectors are aligned. After the data are synchronized, they are processed the same way as described in section 2.1 to the step of discrete Fourier-transformation resulting in the matrix of complex Fourier-coefficients. The correlation process is carried out on these complex matrices. Let us denote these two matrices by s_1 and s_2 respectively. The correlation matrix, c , can be calculated in time-frequency space, using the following expression:

$$c(m, n) = \sqrt{\text{fracs}_1(m, n) s_2^*(m, n) + s_1^*(m, n) s_2(m, n) 2} \quad (6)$$

where s_i^* is the complex conjugate of s_i . Note, that if $s_1 = s_2 = s$ (i.e. single detector case), c is the absolute value of the complex s matrix, thus we get back the input for the single datastream process.

In principle true GW signals present in the coherent datastreams are correlated and thus give rise to positive values in the correlation matrix. On the other hand, noises in the two datastreams are uncorrelated and the corresponding correlation coefficients are

randomly distributed around zero. Therefore negative values and the lower portion of the positive values in the distribution of the correlation coefficients can be attributed to noise and can be changed to the zero level during image processing to speed up processing.

The resulting ROC-curves of the Locust and Hough methods in case of a multiple datastream search and for the same injected signals as for the single detector case are given in fig.(4).

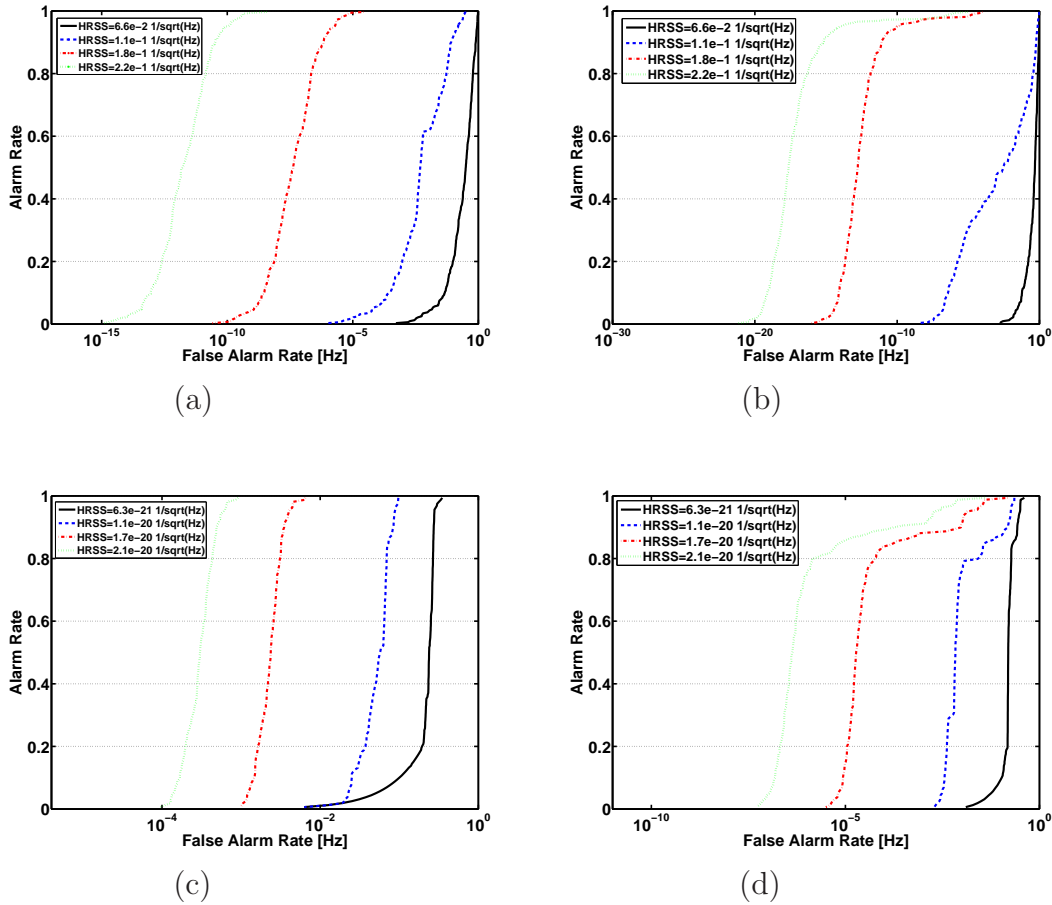


Figure 4. ROC curves of multiple datastream searches. a:white noise/Locust, b:white noise/Hough, c:modified LIGO/Locust, d:modified LIGO/Hough.

5. Conclusion

We have examined two methods to search for quasi-monochromatic gravitational wave signals in datastreams of interferometric gravitational wave detectors. Both algorithms are applied in time-frequency space. The so called Locust algorithm uses local wandering, searching for traces of local maxima in spectrogram of input data. The Hough method is based on a generalized Hough transform, capable of recognizing polynomial curve-like features in the noisy environment of a spectrogram.

Performance measures of these algorithms are illustrated in the context of the van Putten model of long gamma ray bursts and using gaussian white noise and also LIGO-like noise. We characterized the search sensitivity of the two algorithms by mapping Receiver Operating Curves for various signal amplitudes.

As the Locust algorithm uses local wandering, the Hough algorithm has the relative advantage of higher robustness to trace discontinuities. The Locust algorithm is significantly faster and is more general in the sense that it does not require any pre-assumptions on the function describing time evolution of signal frequency. Applying the two algorithms in parallel in one search process provides an opportunity to overcome both above mentioned relative disadvantages for a price of execution speed.

Search methods described in this paper in principle are capable of processing both single and multiple datastreams of gravitational wave detectors. Using the correlation matrix in further steps of search process increases search sensitivity of our methods.

6. Acknowledgements

The authors are grateful for the support of the United States National Science Foundation under cooperative agreement PHY-04-57528, Columbia University in the City of New York and Eötvös University in Hungary. We are grateful to the LIGO collaboration for their support and in particular to P. Shawhan.

The authors gratefully acknowledge the support of the United States National Science Foundation for the construction and operation of the LIGO Laboratory and the Particle Physics and Astronomy Research Council of the United Kingdom, the Max-Planck-Society and the State of Niedersachsen/Germany for support of the construction and operation of the GEO600 detector. The authors also gratefully acknowledge the support of the research by these agencies and by the Australian Research Council, the Natural Sciences and Engineering Research Council of Canada, the Council of Scientific and Industrial Research of India, the Department of Science and Technology of India, the Spanish Ministerio de Educacion y Ciencia, The National Aeronautics and Space Administration, the John Simon Guggenheim Foundation, the Alexander von Humboldt Foundation, the Leverhulme Trust, the David and Lucile Packard Foundation, the Research Corporation, and the Alfred P. Sloan Foundation.

This paper has been assigned LIGO Document Number LIGO-P070025-00-Z.

7. References

- [1] S.A. Hughes, S. Marka, P.L. Bender and C.J. Hogan, Proceedings of the 2001 Snowmass Meeting **eConfC010630**, P402 (2001).
- [2] Abbott B. et al., Nuclear Instruments and Methods in Physics Research A **517**, 154 (2004).
- [3] D. Sigg and the LIGO Science Collaboration, Classical and Quantum Gravity **23**, 51 (2006).
- [4] Acernese, F. et al., Classical and Quantum Gravity **23**, S63 (2006).
- [5] Takahashi, R. et al., Classical and Quantum Gravity **21**, S403 (2004).
- [6] Lück, H. et al., Classical and Quantum Gravity **23**, S71 (2006).
- [7] L. Bildsten, Astrophysical Journal **501**, L89 (1998).

- [8] D.I. Jones and N. Andersson, *Mon. Not. R. Astron. Soc.* **331**, 203 (2002).
- [9] B. Abbott and the LIGO Science Collaboration, *Physical Review D* **69**, 082004 (2004).
- [10] P.R. Brady, T. Creighton, C. Cutler and B.F. Schutz, *Physical Review D* **57**, 2101 (1998).
- [11] P.R. Brady and T. Creighton, *Physical Review D* **61**, 082001 (2000).
- [12] C. Cutler, I. Gholami and B. Krishnan, *Physical Review D* **72**, 042004 (2005).
- [13] Krishnan, B. et al., *Physical Review D* **70**, 082001 (2004).
- [14] B. Abbott and the LIGO Science Collaboration, *Physical Review D* **72**, 102004 (2005).
- [15] S. Frasca, *International Journal of Modern Physics D* **9**, 369 (2000).
- [16] B. Krishnan and the LIGO Science Collaboration, *Classical and Quantum Gravity* **22**, S1265 (2005).
- [17] C. Palomba, P. Astone and S. Frasca, *Classical and Quantum Gravity* **22**, S1255 (2005).
- [18] A.M. Sintes and B. Krishnan, *Journal of Physics: Conference Series* **32**, 206 (2006).
- [19] Kouveliotou, C. et al., *Astrophysical Journal* **413**, L101 (1993).
- [20] Mohanty, S. et al., *Classical and Quantum Gravity* **21**, S1831 (2004).
- [21] S. Marka and L. Matone, *AIP Conference Proceedings* **836**, 605 (2006).
- [22] M.H.P.M. van Putten, *Astrophysical Journal Letters* **575**, L71 (2002).
- [23] H.P.M. van Putten, "Gravitational Radiation, Luminous Black Holes and Gamma-Ray Burst Supernovae", Cambridge University Press (2005).
- [24] H.P.M. van Putten, *Physical Review D* **69**, 044007 (2004).
- [25] H.P.M. van Putten, *New Astronomy* **11**, 619 (2006).
- [26] J. Lense and H. Thirring, *Phy. Z.* **19**, 156 (1918).
- [27] P.V.C. Hough, *International Conference on High Energy Accelerators and Instrumentation*, CERN (1959).
- [28] <http://www.ligo.caltech.edu/docs/G/G060054-00/G060054-00.pdf>
- [29] R.W. Hamming, "Digital Filters", Prentice-Hall (1983).
- [30] F.J. Harris, *Proceedings of the IEEE* **66**, 66 (1978).
- [31] S.K. Chatterji, "The search for gravitational wave bursts in data from the second LIGO science run", PhD dissertation, Massachusetts Institute of Technology (2005).
- [32] D. Sigg, *Classical and Quantum Gravity* **23**, S51 (2006).
- [33] LIGO Scientific Collaboration, *Physical Review D* **72**, 062001 (2005).